Effect of drying procedures on pore structure and phase evolution of alkali-activated cements

Zuhua Zhang [1, 2]*, Yingcan Zhu [1], Huajun Zhu [3]**, Yu Zhang [4], John L. Provis [5], Hao Wang[1]

1. Centre for Future Materials, University of Southern Queensland, Toowoomba, QLD 4350, Australia

2. Key Laboratory for Green & Advanced Civil Engineering Materials and Application Technology of Hunan Province, College of Civil Engineering, Hunan University, Changsha 410082, China

3. Key Laboratory for Advanced Technology in Environmental Protection of Jiangsu Province, Yancheng Institute of Technology, Yancheng, Jiangsu 224051, China

4. State Key Laboratory of Materials-Oriented Chemical Engineering, College of Materials Science and Engineering. Nanjing Tech University, Nanjing 211816, China

5. Department of Materials Science and Engineering, University of Sheffield, Sheffield S1 3JD, UK

Corresponding authors: <u>Zuhua.Zhang@usq.edu.au (Z.Z.)</u>; <u>Hjzhu2008@ycit.edu.cn</u> (H.Z.)

Abstract: This study reports the effects of different drying procedures on the pore determination and phase evolution of alkali-activated cements based on metakaolin (AAMK), fly ash (AAFA) and slag (AAS), as characterized by N_2 adsorption and XRD and FTIR analysis, in comparison with ordinary Portland cement (OPC) paste. The selected drying methods are: (1) 65°C/24 h vacuum drying, (2) 105°C/24 h oven drying, (3) solvent-exchange with ethanol for 3 days then 50°C/24 h oven drying, and (4) freeze-drying with liquid nitrogen. The pore structures of AAMK and AAFA, with zeolite-like sodium aluminosilicate gel phases and little bound water, are less sensitive to drying conditions than are AAS and OPC, which consist of calcium (alumino)silicate hydrates. The drying procedures have less impact on the phase compositions of alkali-activated cements than OPC in general. Nonetheless, caution must be applied in selection of appropriate drying procedures to obtain reproducible and meaningful information regarding the pore and phase structure of alkali-activated cements.

Keywords: alkali-activated cement (AAC), geopolymer, pore structure, drying, gas adsorption.

1. Introduction

Microstructural characterization of cements and concretes is essential for the understanding of their macrostructural properties and long-term performances [1]. Among different measured properties,

pore structural and phase composition characterizations are important for the determination of durability and stability for concretes. As is the case for Portland cement-based mortars and concretes, their pore structure determines the transport of potentially aggressive species into the concrete matrix, which further affect the chemical stability of the binding phases and the reinforcement bars [2]. For alkali-activated cements (AACs), as relatively new compared to PC materials, characterization of pore structure and phases are also important for the assessment of their durability, which is particularly required as there is limited long-term practice data to track. Although some AAC phases are more stable in aggressive environments than OPC hydration products [3, 4], alkali-activated metakaolin and fly ash geopolymers have been observed to have higher chloride permeability than OPC because of their more porous nature [5, 6], as the alkali aluminosilicate gel phases which dominate their structure do not bind water in the same way as do calcium silicate hydrate-type phases [7].

Accurate measurement of pore structure of AACs is essential for their permeability, and other characteristics relevant to durability, to be fully understood. However, as noted above, the reaction products of alkali-activation are different in composition and microstructure from OPC hydration products. This means that when different binders are exposed to a particular drying condition to remove evaporable (free) water for porosimetric measurement, their pore structure may be changed in a manner which is dependent on their nature, and thus not consistent across all binder compositions. This has been found in OPC based concretes; by adding fly ash into OPC concrete, the pore structure become less sensitive to humidity because of the change in the composition of hydration products [8]. Therefore, caution must be taken in the selection of an appropriate drying method to retain pore structure to the greatest possible extent, and the most appropriate method to apply for alternative binders, such as AACs, may differ from that which is optimal for OPC-based binders.

There are four common drying methods of hydrated cement samples: (1) oven-drying at 50-105°C, (2) vacuum-drying, (3) freeze-drying (sublimation) and (4) solvent replacement drying. Several studies have compared the effect of drying techniques on the measurement of OPC binder and concrete [1, 9-13]. Selection of a 'suitable' drying method is required for each particular purpose and type of characterization [13]. For the purpose of measuring pore structure, the general indication from the existing studies of OPC based materials is that oven drying at 105°C leads to overestimation of pore volume and radius because of the loss of nonevaporable water from ettringite and C-S-H gel; vacuum drying and solvent replacement drying at milder temperatures

2

around 40-60°C are relatively less destructive. However, these three methods may lead to misleading information for a large capillary porosity because of the capillary stress, desiccation of cement hydrates (ettringite, AFm, C-S-H) and potential microcracking, as determined by mercury introduction porosimetry (MIP) [9]. Freeze-drying is thought to be less destructive than oven drying methods, and suitable for MIP study [9]; however, more severe damage to microstructure of OPC binder was also reported when using this method rather than acetone quenching [14].

There is only limited information in the open literature on the comparison of the changes introduced by drying methods on the phase and pore structure of AACs. Ismail et al. [15] compared the 60 °C oven, -85 kPa vacuum and acetone exchange drying methods on the pore structure (as determined by nitrogen sorption) of alkali-activated slag and slag/fly ash blends, and found that oven drying of these pastes had a more detrimental effect than vacuum and acetone drying in terms of increasing the pore volume in the micropore region; all the drying methods reduced the total pore volumes, which is different from the case for OPC systems where pore volumes usually increase after drying [14]. Those authors recommended that to avoid alternation of gel structure or pores as far as possible, it is desirable to apply the acetone drying method to AACs based on blast furnace slag, and to apply either vacuum or acetone methods to AACs based on lower-calcium precursors. Yang et al. [16] recently reported the significance of preconditioning of alkali-activated slag (AAS) samples for air permeability testing because of the effect of moisture content, which is only removed after 10 days of drying at 40°C and relative humidity 35%. This provides further evidence of the high sensitivity of AAS materials to drying conditions.

In this study, we aim to understand the effect of drying methods on the measurement of pore structure and any associated phase changes in three AACs: alkali-activated metakaolin (AAMK), alkali-activated fly ash (AAFA), and AAS. A gas sorption method using nitrogen as a probe molecule is adopted in this study. Mesopores with diameters of 2-50 nm are particularly of interest as they are expected to be critical in controlling the transport processes of liquid and external aggressive ions [17]. Exploration of the nature of these structures, and their sensitivity to drying techniques, is fundamental to the wider study of durability-relevant material characteristics in AACs.

2. Materials and methods

2.1 Materials

Three types of AACs were synthesised based on metakaolin, fly ash and granulated blast furnace slag. The metakaolin was supplied by Taojinfeng New Materials Ltd, Fujian, China. It was a product of finely powdered kaolin heated at 800°C for 2 hours. The fly ash and slag were obtained from a local concrete supplier in Yancheng, Jiangsu, China. The fly ash was grade I according to the Chinese standard GB/T1596-2005 [15]. The characteristics of grade I fly ash include >88% of particles finer than 45 μm, water demand less than 95%, loss on ignition less than 5%, and water content less than 1%. For comparison, OPC paste was also prepared, using grade 52.5 I Portland cement, supplied by Conch Cement Company Limited, China. The chemical compositions of the metakaolin, fly ash, slag and cement were determined by X-ray fluorescence (XRF) method and the results are given in Table 1.

Table 1. Compositions (mass%) of raw materials as determined by XRF, represented on an oxide basis. LOI is loss on ignition at 1000°C.

Composition	SiO_2	Al_2O_3	Fe_2O_3	CaO	MgO	K_2O	Na_2O	SO_3	LOI	*sum*
Metakaolin	55.9	42.2	0.4	0.0	0.0	0.3	0.3	0.0	0.6	99.7
Fly ash	54.3	33.3	4.4	5.2	0.6	0.8	0.4	0.1	1.1	100.1
Slag	35.5	20.6	1.4	32.4	5.8	0.3	0.5	0.7	1.9	99.1
Cement	20.3	5.5	3.3	64.9	1.6	0.3	0.3	1.0	2.3	99.5

The activator used for all three types of AACs was a sodium silicate solution with a modulus (SiO_2/Na_2O molar ratio) of 1.5 and a concentration of 35 wt.% solids. Firstly, NaOH pellets was dissolved in distilled water to reach concentration of 12 mol/L and cooled to room temperature. Then the NaOH solution was mixed into a high modulus commercial liquid sodium silicate (Na_2O = 8.3 wt.%, SiO_2 = 29.9 wt.%) and distilled water was used to adjust the mixture to a concentration of 35 wt%. The activator was allowed to equilibrate at room temperature prior to use.

2.2 Preparation of AAC and cement pastes

AAC pastes were prepared by adding the activator gradually to the powders in a mixing bowl. Due to the different particle finenesses and morphologies of the powders, the three AACs required different liquid/solid ratios to achieve desirable workability for casting. A mini-slump testing was conducted using a steel cylindrical cone with internal diameter of 50 mm and height of 50 mm. The slump target for the three type of AACs was set to be 130-140 mm. At this workability, the mix proportions are given in Table 2; the Na_2O/solid material ratio was 4.5% in AAS, which is relatively lower than in AAMK and AAFA due to the higher reactivity of the slag than the other precursors. Here the definition of solid material includes both the aluminosilicate powder and the dissolved solids in the activator solution, i.e. Na_2O and SiO_2.

Table 2.   Mix proportions and compressive strengths (mean and standard deviation among 6 replicates) of AAC and OPC pastes.

Specimens	Metakaolin (g)	Fly ash (g)	Slag (g)	Portland cement (g)	Activator (g)	H_2O (g)	Total w/s ratio	28-day compressive strength (MPa)	True density (g/cm³)
AAMK	100	0	0	0	65	0	0.37	46.0±1.0	1.96
AAFA	0	100	0	0	45	0	0.25	54.8±4.8	1.95
AAS	0	0	100	0	35	10	0.28	101.1±5.0	2.22
Cement	0	0	0	100	0	32	0.32	78.8±7.2	2.08

The homogeneously pastes mixed mechanically were transferred to steel moulds ($20 \times 20 \times 20$ mm), filling the moulds in thirds and tamping 20 times for each layer, then vibrating for 5 min to remove large air bubbles. The AAC samples were wrapped with nylon sheets and cured at 20±1°C for 1 day, demoulded, further cured at 50±2°C for 2 days in a sealed container and then aged at RH>95%, 20±1°C for 28 days. The OPC cement paste was prepared at water/cement (w/c) ratio of 0.32, which gave high workability and allowed easy casting. The casting procedure was the same as for AACs, followed by standard curing for 24 hours, demoulding, then plain water bath curing at 50±1°C for 28 days, and finally the material was equilibrated at standard curing conditions for 48 hours prior to testing. This elevated temperature bath curing was chosen to obtain high maturity of the samples. The matured AAC and cement paste cube specimens were tested for compressive

strength on a RG-3010 universal mechanical testing machine, at a load rate of 0.5 mm/min. For each mix, six replicate specimens were tested to give the mean and standard deviation in compressive strength, which are given in Table 2. The true densities of AAMK, AAFA, AAS and PC pastes were determined by kerosene substitution method [18].

2.3 Drying and characterization of its effects

In preparing samples for drying, crushed cube samples after mechanical testing were used. To eliminate any potential effects due to surface carbonation, the inner parts of fractured samples were collected and crushed into particles with a minimum dimension of 1-2 mm. This size was selected based on experience from previous studies [10]; grinding into finer particles may affect the determination of surface area and pore size distribution as artificial surface is mechanically generated; in the size range 1-2 mm it is believed that the size effect is limited [19]. The crushed samples were blown using compressed air to remove adhered fine particles from the surface.

Four drying methods were used:

(1) 65VD - vacuum drying at 65°C: samples were placed in a vacuum drying chamber for 24 hours at 133 Pa absolute pressure;

(2) 105D - oven drying at 105°C: samples were placed in a conventional laboratory oven for 24 hours;

(3) A50D - ethanol replacement and oven drying at 50°C: samples were soaked in ethanol for 3 days (which is believed to be sufficient for complete exchange in Portland cement [13]), followed by drying in a conventional laboratory oven at 50°C for 24 hours;

(4) FD - freeze-drying: samples were frozen by immersion in liquid nitrogen for 10 min. This quick freezing process at very low temperature (-195°C) allows generation of ice microcrystals in samples, which were then removed under vacuum (133 Pa absolute pressure) at 60°C for 6 hours.

Considering the possible absorption of moisture from air, each dried sample once removed from the respective drying conditions was immediately stored in a dried glass bottle with a seal, and kept in a desiccator containing freshly dried desiccant. The storage time of the dried samples was as

short as possible prior to characterization. Undried samples stored under ambient conditions, $20\pm3°C$ and RH ~40%, were also measured. Because of the relatively low RH, the free water in the crushed particles will evaporate to some extent, leaving some of the capillary and maybe a few nanosized pores open.

To examine the effects of drying on water retention, pore measurement and binder phase, thermogravimetric analysis (TGA) was performed using a TA Instruments Q500. For each test, 10-20 mg of ground samples was heated from room temperature to 1000°C at 10°C/min. High purity dry nitrogen flowing at 16 mL/min was used for the sample purge. The nitrogen adsorption/desorption for the dried samples (1.5-2.0 g) was performed on a TriStar II 3020 instrument to determine their pore structure and surface areas. Regardless of prior drying treatment, all samples tested by nitrogen sorption were de-gassed according to the standard protocol for this technique, which is heating to 105°C for 2 hours. Although this procedure introduced complexity to the interpretation of the effects of the different drying procedures, it is essential to de-gas the sample prior to analysis, and this short-term heating was selected in preference to a low temperature long term vacuum process [15]. The Barrett-Joyner-Halenda (BJH) [20] calculation results obtained from the desorption branch of the isotherms are reported, including pore size distribution and cumulative pore volume.

XRD analysis for finely ground sample powders was performed using a DX-2700 X-ray diffractometer with Cu Kα radiation, operated at 40 kV and 30 mA, with a step size of 0.03° and count time of 0.3 s per step from 5° to 80° 2θ. Attenuated total reflectance (ATR)-Fourier transform infrared spectroscopy (FTIR) was used to detect any influence of the drying methods on the vibrational spectra of the samples, while avoiding the preparation of KBr disks which would induce further drying.

3. Results and discussion

3.1 TGA

Figure 1 shows the mass loss as determined by TGA for the three types of AACs and the OPC paste, after curing and drying by the four methods described above. One control sample for each mix type, to which no drying procedure (other than ambient storage) was applied, was used to compare with the others, and is marked 'undried' in the plots. The four cements exhibit different weight loss trends because of the distinctive natures of the binding gels present in each. For AAMK

(Fig.1A and 2A), the undried sample and the FD sample have very similar mass loss profiles, and the 65VD and A50D samples are also similar in terms of the observed mass loss trend. This enables the identification of two groups of methods which each have similar efficiencies in removing water: undried or freeze-drying, *vs*. vacuum drying or ethanol replacement drying. The undried and freeze-dried samples lose more water during the TGA testing (i.e. have had less water removed by drying processes) than those treated under vacuum or by solvent exchange. The 105D sample loses the least amount of water in TGA, indicating that this has been the most aggressively dried prior to testing.
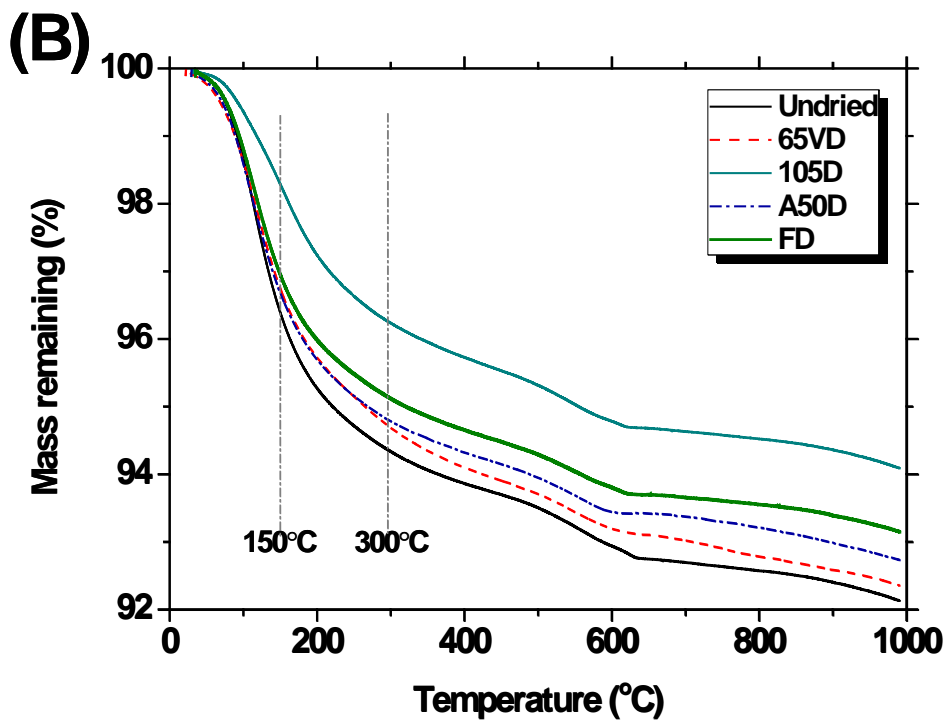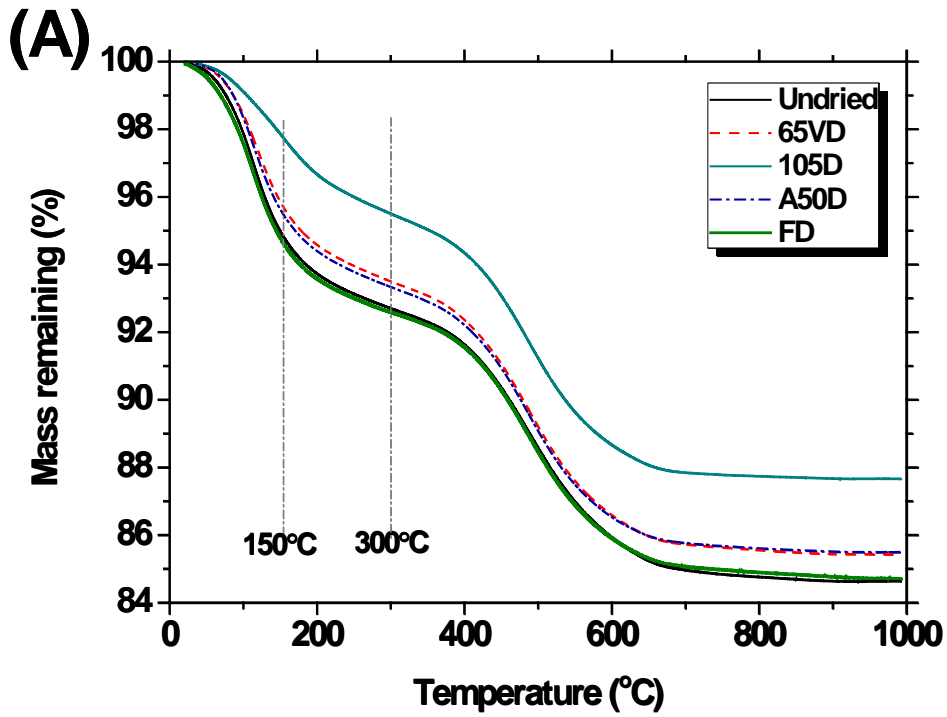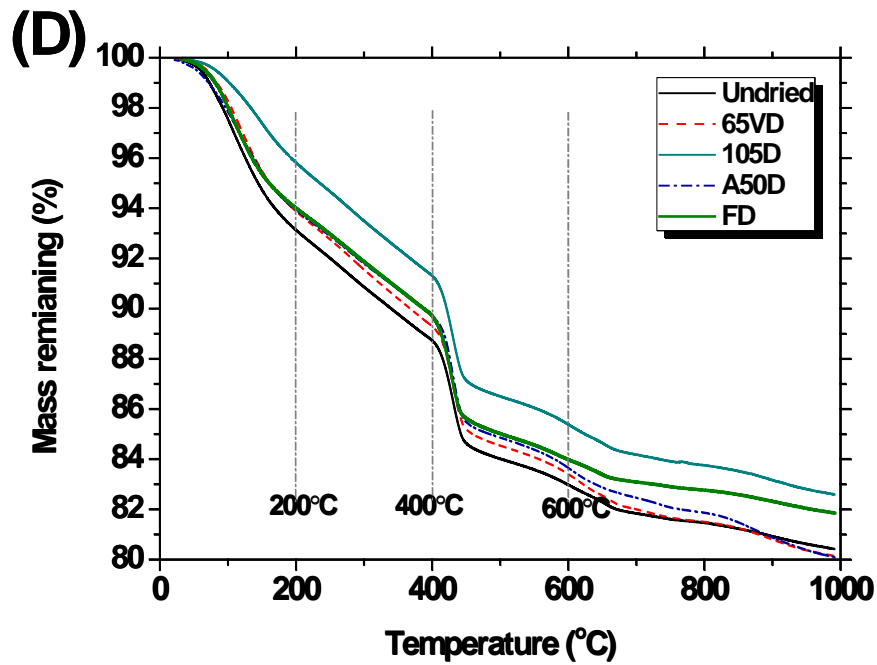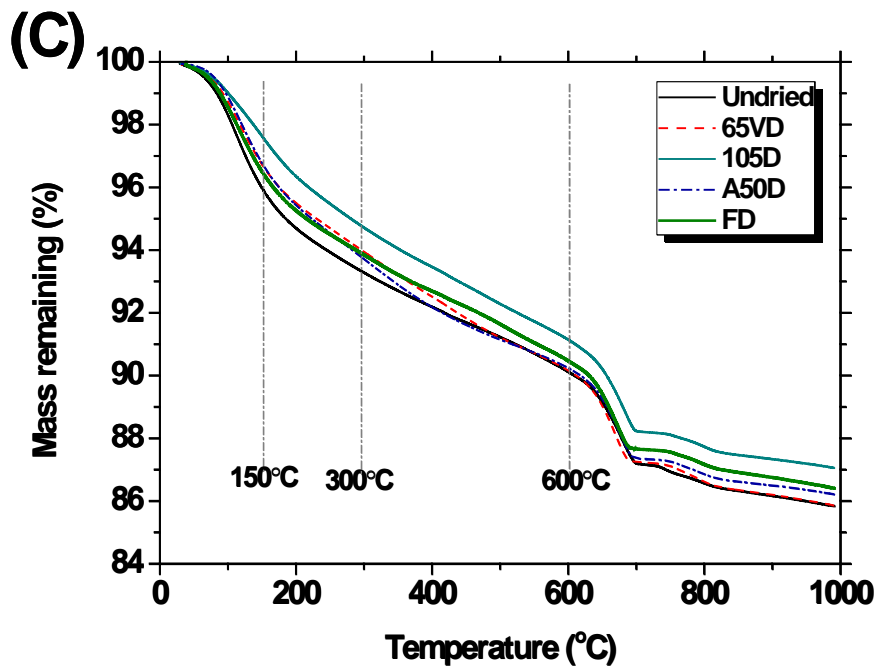
Fig.1. TGA curves for pastes after various drying procedures: (A) AAMK, (B) AAFA, (C) AAS, and (D) OPC.

The major difference in weight loss profile among the five AAMK samples occurs before 150°C; after this point, the TGA curves are almost parallel. Water which requires temperatures greater than 150°C to be removed from the binder is evidently too tightly bound to be removed prior to testing by any of the drying methods applied here. If it is assumed that the three regions of weight loss 25-150°C, 150-300°C and 300-600°C are attributed to evaporation of free water, loosely bound water and dehydroxylation of alkali aluminosilicate gels respectively, as was previously determined by other workers [21], the drying methods only significantly affect the loss of free water and part of the loosely bound water. This is indicated by the asymmetric DTG peak of the AAMK sample 105D between 25 and 300°C in Figure 2A, which can be identified to consist of two sub-peaks centered at 117 and 175°C respectively. The DTG peak for dehydroxylation of alkali aluminosilicate gels, i.e. loss of structural water from -Si(Al)-OH, may overlap with the decomposition of any sodium carbonate formed during sampling. However, the sodium carbonate appears only in a very minor amount, and this will be supported by further analysis below. The small weight loss above 600°C shown in DTG is more likely due to calcination of the residual kaolinite in the metakaolin [22, 23], rather than further dehydroxylation of gel reaction products, because (1) there is still a certain amount of residual kaolinite which has not been completely transformed into metakaolin within the precursor, as evidenced by XRD results in the following sections; (2) the dehydroxylation of alkali aluminosilicate geopolymeric gels is usually complete before 600°C [24, 25]. Further evidence for this is also seen in Fig.2B, if it is assumed that the thermal stabilities of the aluminosilicate gels are similar in AAMK and AAFA. For both Na-based and K-based AAMK, the dehydrated gel phases are stable in mass past 600°C as they have almost completely lost all structural water [26, 27].
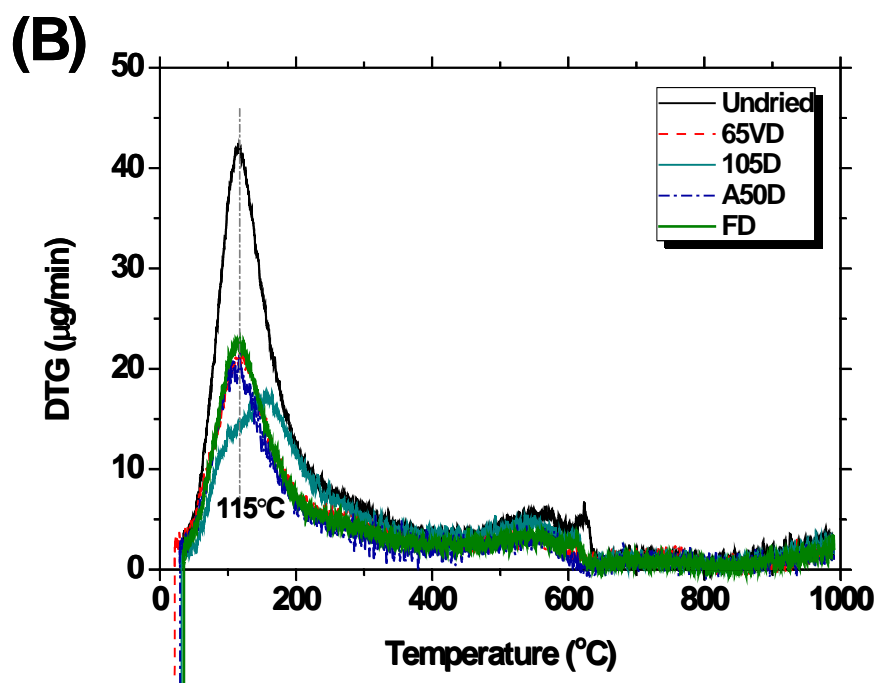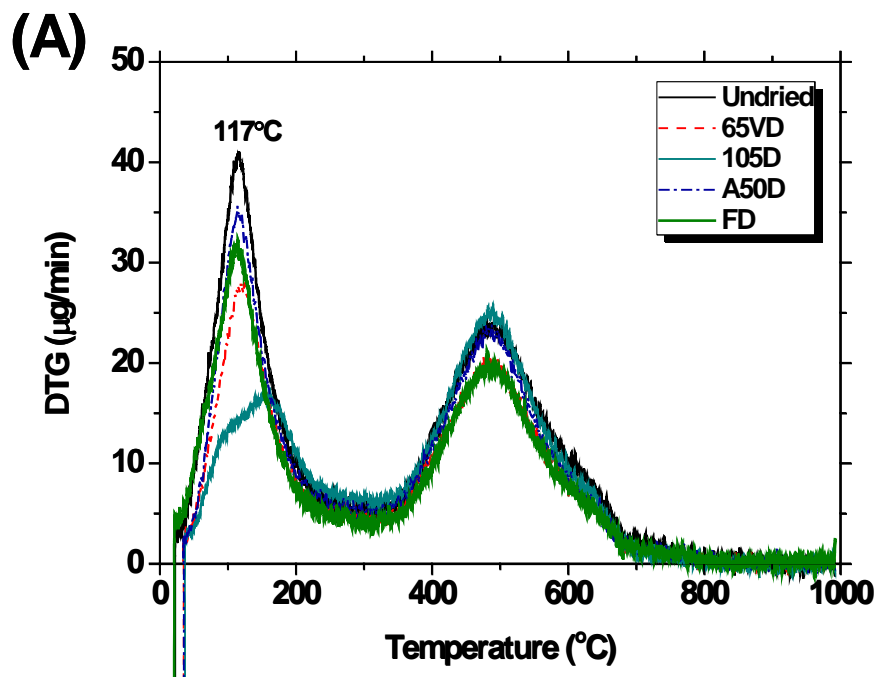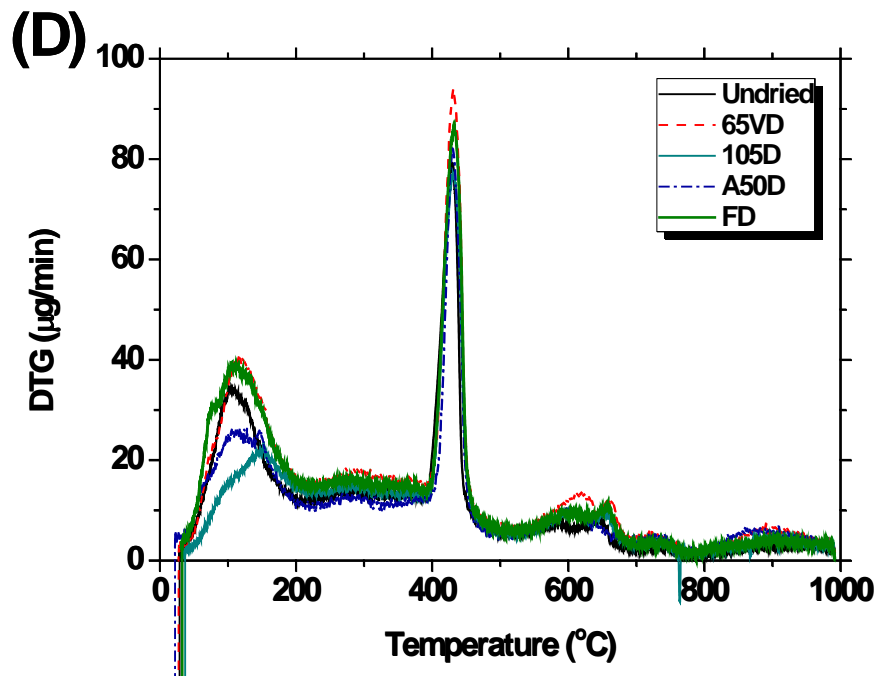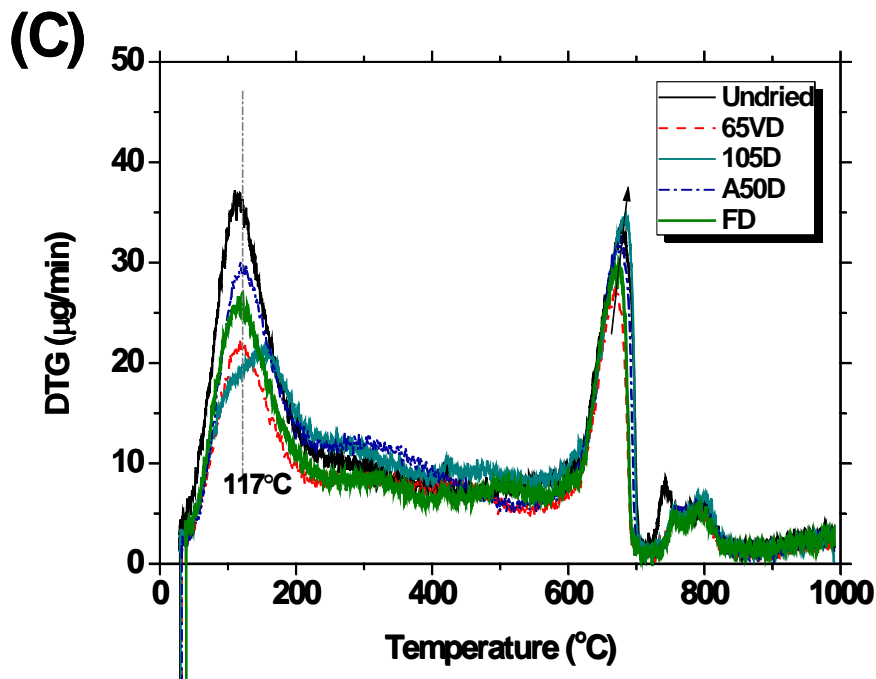
Fig.2. DTG curves of hydrated AAC and cement pastes after various drying procedures: (A) AAMK, (B) AAFA, (C) AAS and (D) OPC.

For AAFA, the trends are similar: the largest mass loss during TGA analysis (Figure 1B) occurs in the undried sample, and the smallest again in the 105D sample. The 65VD and A50D samples show similar drying efficiencies in the data up to 300°C, and the difference between them is observed in

terms of behavior between 300 and 600°C. This means that the two drying methods have similar degrees of effectiveness in removing free and loosely bound water. A difference between AAMK and AAFA is that FD seems more efficient for drying of AAFA. When a geopolymer sample is immersed in liquid nitrogen (−196°C), free water freezes in its pores and becomes ice. After 6 h of vacuum freeze drying, water is removed effectively from AAFA samples but still retained to some extent in AAMK. This may indicate that the microstructure of AAMK restricts the sublimation of water, or may be related to the significantly larger water content of this mix (Table 1). It may be that a longer (>6 h) vacuum period is required to complete the sublimation and escape of water from AAMK. However, for AAFA, the FD procedure looks very efficient, although induces less drying than 105D.

Comparing the TGA profiles of the five AAFA samples in Figure 1B, the major difference still occurs before 150°C, which again confirms that choosing the four drying procedures mainly affects the removal of free water and partial loosely bound water, but with some minor differences in other water environments. In the TGA curves there is still some mass loss (about 1%) above 600°C, which was also shown in a previous study [28]; the DTG curves show a weak peak at 600-800°C and an increase of weight loss rate at >800°C. The former is likely due to the decomposition of carbonates, which could be a mix of calcium carbonates resulting from the source materials [29] and sodium carbonates which are formed during demolding and sampling. The relatively more distinguished peak at 600-650°C of the undried sample indicates that the more rapid carbonation occurring under the ambient storage conditions. The small weight loss above 800°C is probably due to some degree of alkali volatilization at these high temperatures [30].

For AAS, from the TGA curves (Figure 1C) it is seen that the smallest mass loss upon heating occurs in the 105D sample, which means that drying at 105°C for 24 h appears to be the most efficient method of removing water, although its influence on the integrity and structure of the material after drying remains to be determined. The total mass loss values for the undried and 65VD samples are the same; this indicates that vacuum drying removes rather a limited amount of water from the AAS. There is a relatively larger weight loss in the 65VD and A50D samples between 300 and 400°C; the vacuum conditions and solvent replacement enable more retention of structural water in AAS than does oven drying. The loss of structural water from calcium aluminosilicate hydrate gels such as those which dominate the structure of AAS is generally completed before 400°C [31]; however, due to the complexity of the reaction products, it is difficult to determine the exact quantity of structural water that was present in this gel before any drying

treatment was applied [32-33]. From the DTG curves (Figure 2C), it is noted that after the first mass loss peak at 25-200°C, there is significant ongoing mass loss continuing from 200 to 600°C, overlapping the peak at 650-700°C, and followed by minor peaks at 700-800°C. The drying procedures significantly affect the lower-temperature peak, which represents the evaporation of free and loosely bound water; especially, drying at 105°C removes a large amount of free water as shown by the asymmetry of this peak in the data for 105D. The weight loss at 200-600°C is due to the decomposition of C-A-S-H and additional layered double hydroxide reaction products (mainly in the hydrotalcite family) [33], and the relatively high rate of mass loss in this range in the A50D sample suggests that the solvent replacement aids the retention of structural water in the gel through drying so that it is able to be measured in the TG analysis. It should be noted that there is not a chemical reaction between the ethanol and portlandite in this system, which means no affection to the determination in this temperature range [34]. The solvent lessens the deleterious effects of drying on the hydrous gel, aiding the small pores to resist collapse during drying [35]. The peaks at 650-800°C are attributed to the decomposition of calcium carbonates [25, 36, 37], which is further evidenced by the XRD analysis presented below. Overall, for AAS, the most aggressive drying procedure is once more 105D; the other three protocols are almost equivalent in removing free and loosely bound water but have different effects on structural water.

For comparative purpose, the effects of drying procedures on OPC were also recorded; TG data are in Figure 1D and DTG in Figure 2D. From the DTG curves, in the dried samples, there are four weight loss peaks at 25-200°C, 200-400°C, 400-460°C, and 500-800°C, which are attributed to the decomposition of ettringite, decomposition of calcium silicate hydrate (C-S-H), dehydration of $Ca(OH)_2$, and decarbonation of calcium carbonates, respectively [13, 38]. The weak peak appearing after 800°C was also found in other studies [14], but its cause is not clear. The decomposition of C-S-H overlaps with all other phase changes taking place at different temperatures. The 105D procedure significantly affects the weight loss before 200°C, which means the continuous high temperature drying for 24 h has led to the partial decomposition of C-S-H, AFm phases, and ettringite [39]. The effects of the four drying methods on OPC samples are similar to their effects on AAS, but different from AAMK and AAFA, because the chemical nature of the binder gel in AAS is more similar to the C-S-H that forms as an OPC hydration product [32, 40].

3.2 Pore analysis by nitrogen adsorption

Figure 3 presents the pore size (diameter) distributions of AAC and OPC pastes as determined by nitrogen adsorption using the BJH method; the adsorption branch of the isotherms was used to avoid tensile strength effects and potential related misinterpretation [41]. For AAMK, the four drying methods do not alter the pore size distribution significantly. There are two characteristic sizes of pores in AAMK within the size range that is observable by this technique: small pores which appear as a peak at 2.5 nm in Figure 3A, and larger pores which show a broad distribution centered at 20 nm, spanning the range from 4 to 30 nm. The former is attributed to the intrinsic pores formed between sodium aluminosilicate hydrate (N-A-S-H) gel particulates [42]; the larger pores represent the space between gel units, i.e. capillary pores, and are very close to those detected by MIP methods [43, 44]. The pore size distribution is almost constant when drying methods 65VD, 105D and FD are adopted. Only A50D leads to a slight increase of pore volume (Figure 4A). In comparison, the undried sample shows pores over the range of 2 – 70 nm, which are almost the same as the others but in much lower volume. The finding suggests that AAMK gels are not sensitive to differences between the drying methods, at least in the mesopore range, although it is not possible to exclude the possibility that the degassing process which is necessary for nitrogen sorption analysis has masked any differences that may have been present in the as-dried samples.

For AAFA (Figure 3B), the different drying methods show more evident effects on the pore size. There are no clear characteristic sizes to separate gel pores from capillary pores, but rather a broad distribution of pore sizes is centered in the range 4 – 10 nm. The undried sample reaches a maximum in its pore size distribution at 4.0 nm; after drying, it shifts to larger sizes, 5.1 nm for A50D and 6.0-7.5 nm for 65VD, 105D and FD. This indicates that A50D could be the least damaging drying method for AAFA pore structure. It also leads to a slightly higher total measured pore volume according to nitrogen sorption analysis, as can be seen in Figure 4B. Considering the similar results in the AAMK system, it appears that solvent replacement method is a relatively safe and effective approach for drying treatment of low-calcium alkali-activated binders. It removes the pore solution, which contains a considerable amount of dissolved species, and eliminates the effect of their gelling/solidification on pore walls; it also reaches small pores to enable more realistic porosity determinations.
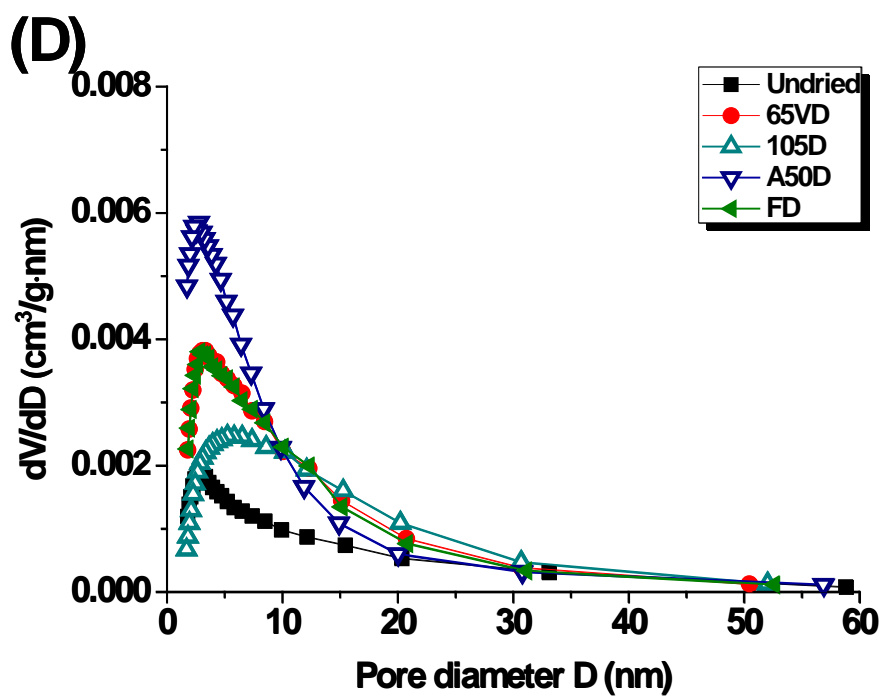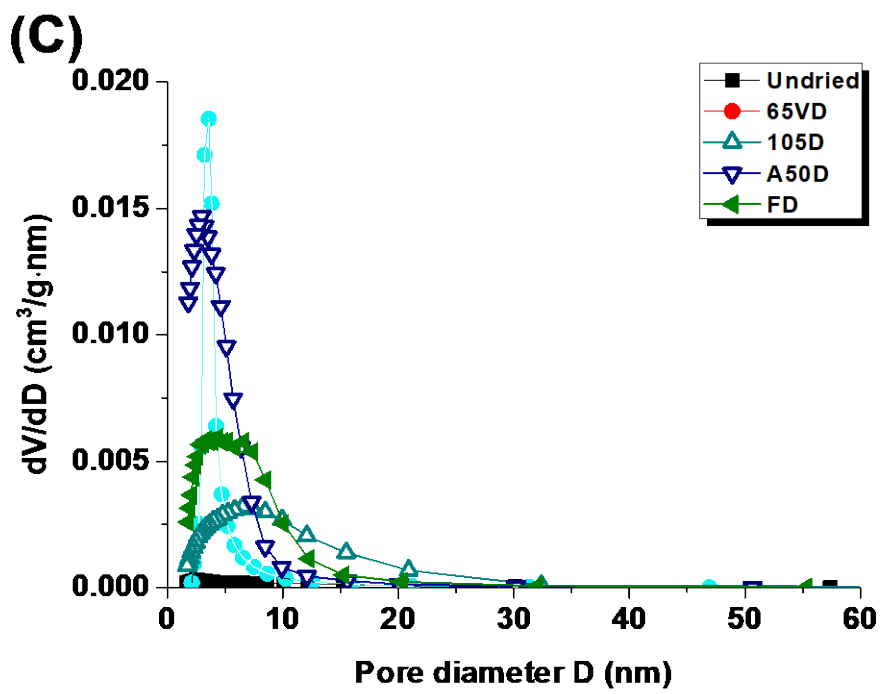
(A)

(B)
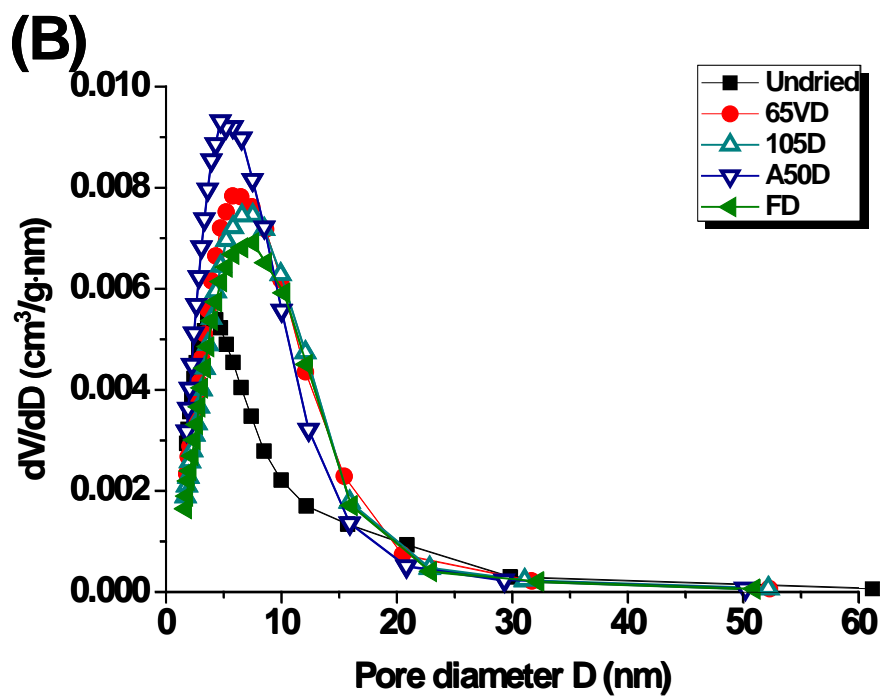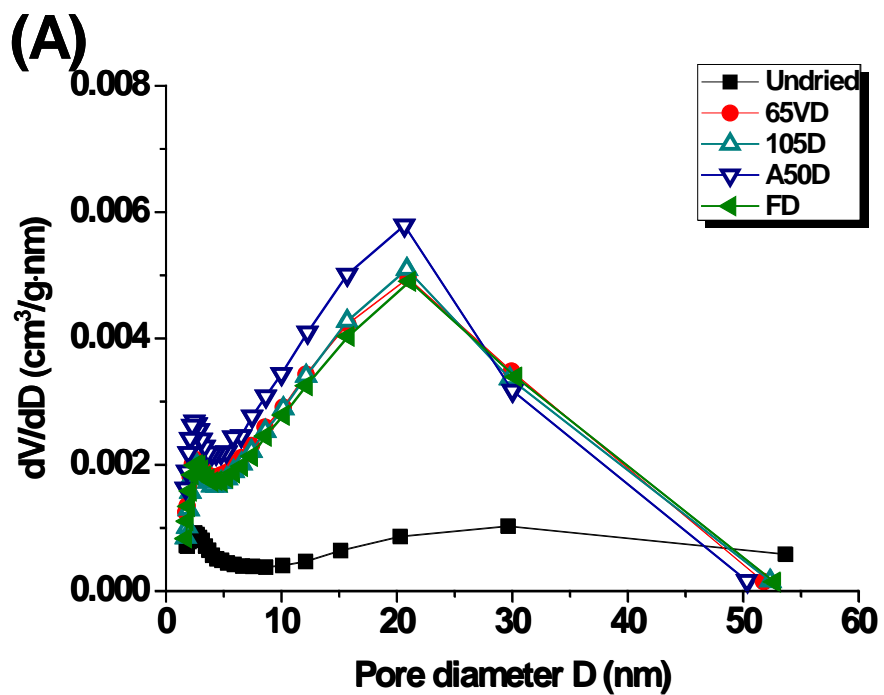
Figure 3.   Pore size distribution (determined by BJH analysis of nitrogen adsorption isotherms) of: (A) AAMK, (B) AAFA, (C) AAS and (D) OPC.

For AAS and OPC pastes, the effect of drying temperatures is much more evident than in the AAMK and AAFA. Figure 3C and D show that oven drying for 24 hours at 105°C (105D) leads to more large pores in the two binders. This is probably due to the decomposition of hydrates and the formation of shrinkage induced microcracks [45, 46]. For AAS, the 65VD procedure leads to the narrowest pore size distribution in the range accessible to the BJH technique, followed by A50D, then FD, and finally 105D gives the broadest. From the cumulative pore volume curves, 65VD reaches more pores that are finer than 5 nm. Solvent exchange with ethanol (A50D) is again proven to be the least damaging drying method used in this study. The volume of pores >5 nm in the A50D sample is the smallest among the dried samples. For OPC, the 65VD and FD samples have almost the same pore size distribution, meaning that the methods appear to be giving comparable results. A50D gives more fine pores while 105D gives more pores larger than 10 nm, indicating that the higher temperature has caused more collapse of the finer pores leading to coarsening. Although the total pore volumes of OPC samples after drying are equivalent in the accessible pore size range, the contribution of the pores >5 nm is in the order 105D>65VD≈FD>A50D. This is generally in agreement with the summary of Zhang and Scherer [13], who stated that 'to preserve microstructure' in OPC, solvent replacement is better than freeze drying, while oven drying is the worst.

These results show that the drying procedures cause evident effects on pore size and volume measurement by gas adsorption, which must be considered for AAS and OPC. The results shown in Fig.4 also explain the extraordinarily low porosities of AAS and AAFA cements and concretes in some published measurements [5, 47]. It is not because of the formation of binder 'without pores', as is sometimes claimed [5], but because of incomplete drying and the difficulty for the intrusion of the probe fluid that is used in the measurement. Selection of a proper drying technique and pore characterization method is essential in truly understanding the pore structure of cements.

The comparison between these four substantially different binders also shows that the low-calcium AACs (AAFA and AAMK) are less sensitive to the drying conditions than the higher-calcium cements. The most important factor in the drying conditions is probably the temperature difference. Despite the decomposition of ettringite in OPC at relatively low temperature (<150°C) as mentioned above, this sensitivity is also related to the nature of the gels, the elemental composition and their nanostructure. The hypothesis is that the thermal stability of the N-A-S-H in AAMK and

AAFA is higher than that of C-A-S-H in AAS and C-S-H in OPC, and this is well supported by evidence from the literature [48, 49].

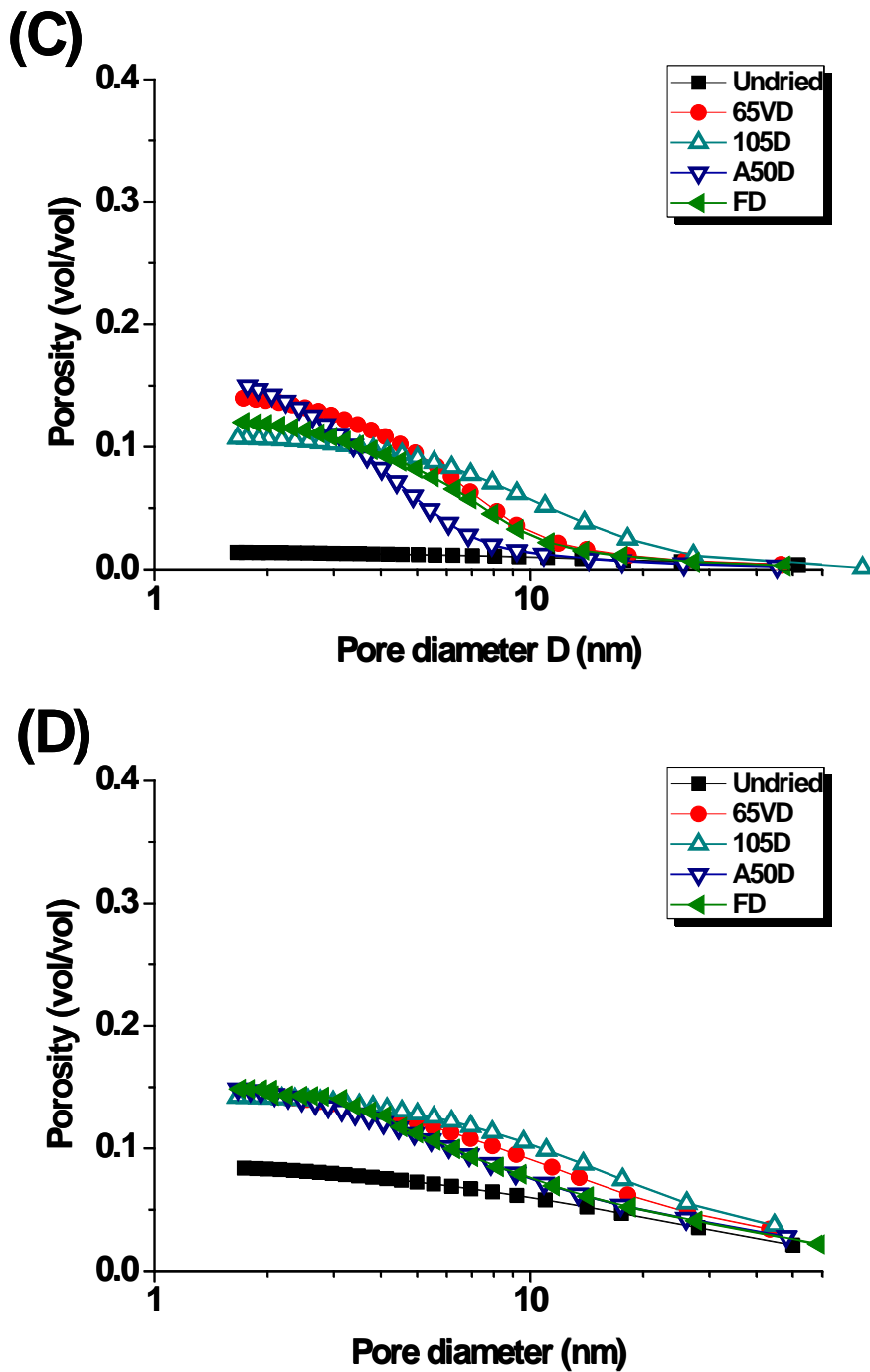**(A)**

(B)

(C)

(D)
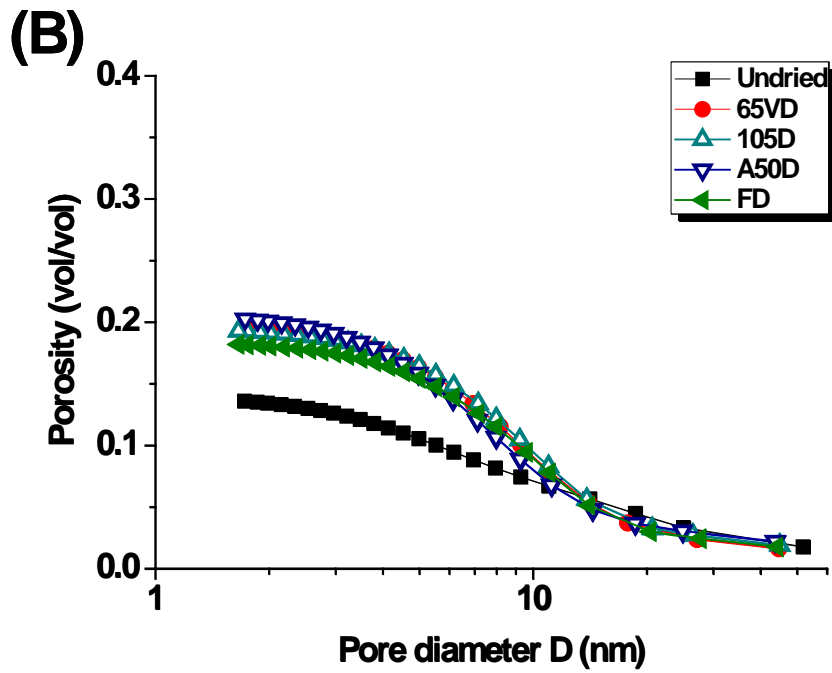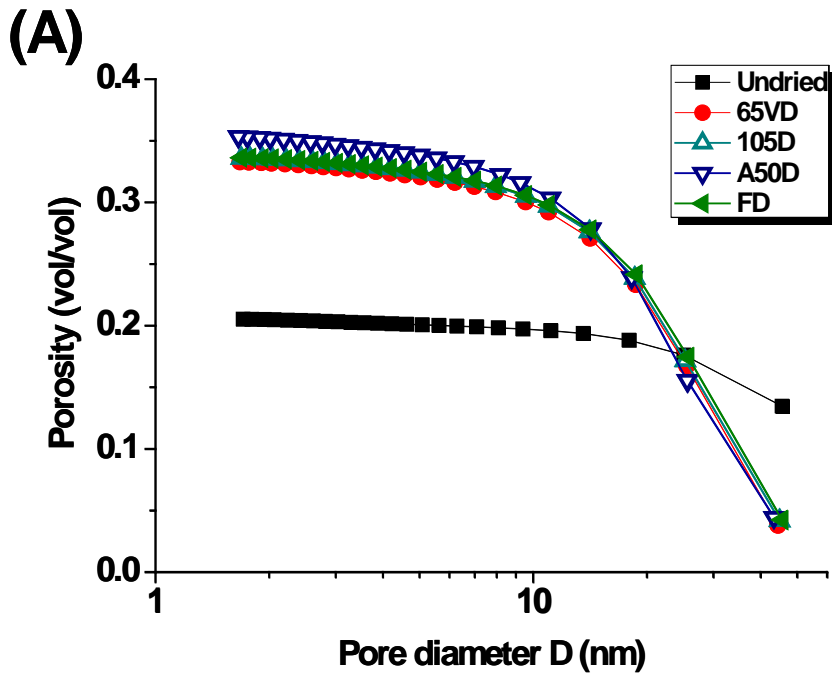
Figure 4.   Porosity (by BJH adsorption) of pastes: (A) AAMK, (B) AAFA, (C) AAS and (D) OPC.

Fig. 5 presents the effects of the drying procedures on the BET surface areas of the AAC and OPC pastes. Surface area of cement is a function of pore volume and pore size, which is also a parameter that can correlate with its durability performance under exposure to aggressive environments [47]. The results shown in Fig.5 confirm that due to the difference between the results obtained following

different drying procedures, caution should be taken in the measurement and interpretation of BET surface areas. In general, the undried samples exhibit the smallest surface areas in each group, while the A50D samples have the largest. As discussed above, the large surface area of samples dried by solvent replacement is related to the lower degree of pore collapse and coarsening enabled by the use of the solvent. As a result, fine pores remain open and accessible. For AAMK and AAFA, the measured surface areas are equivalent after 65VD, 105D and FD drying, but increase by 15% after the A50D treatment. For AAS and OPC, the drying procedures have a very remarkable effect on the surface area; the influence is particularly large in AAS. However, 105D does not lead to higher surface area as compared to other drying procedures; drying at high temperature is expected to cause cracks in the binder [14], but these will not contribute much to surface area because of their large size, and so the collapse of fine pores in this process leads to a reduced surface area in the AAS and OPC pastes.
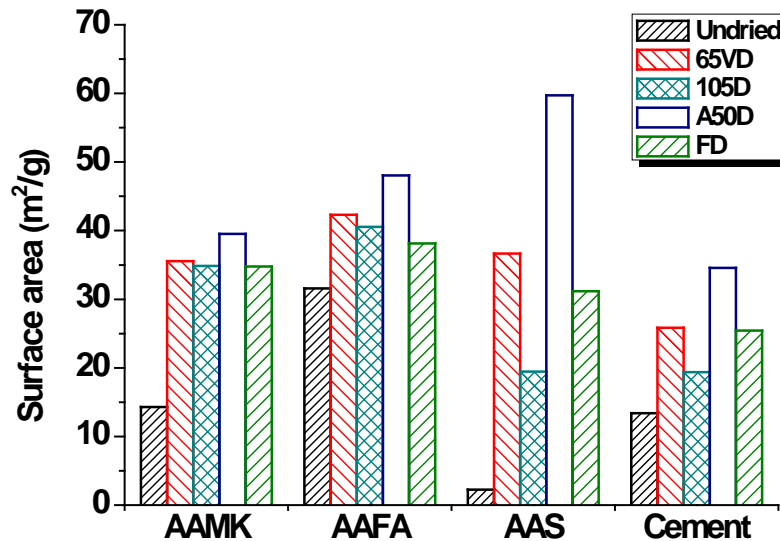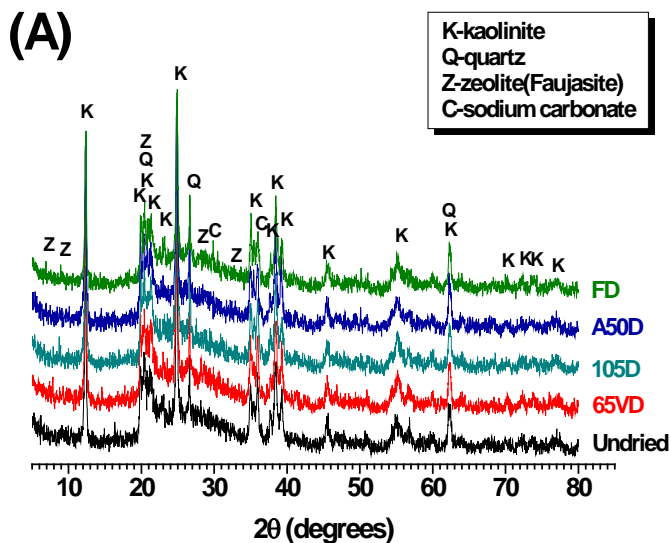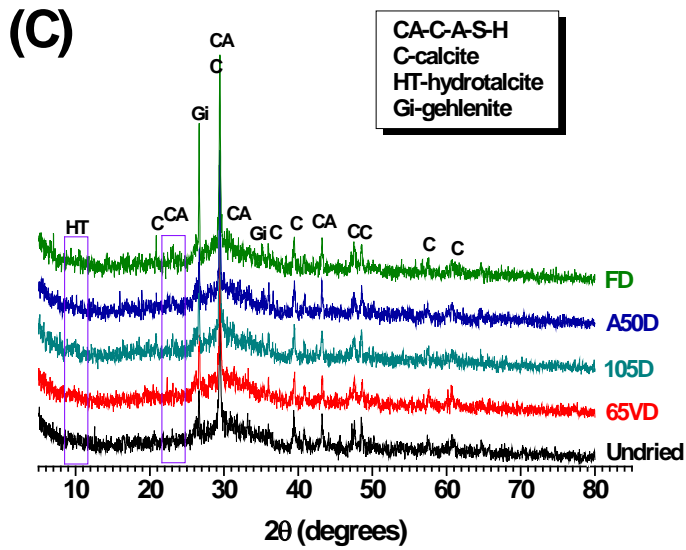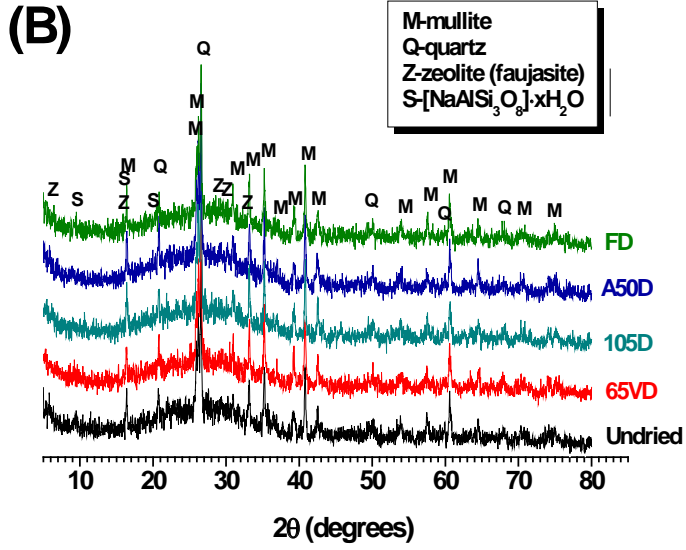

Fig. 5. BET surface areas of dried and undried AAC and cement pastes.

3.3 XRD analysis of phase changes

Fig. 6 shows the effect of the drying procedures on the phase composition of hydrated AAC and OPC pastes. In AAMK (Figure 6A), there are kaolinite ($Al_2O_3 \cdot 2SiO_2 \cdot 2H_2O$, Powder Diffraction File card number (PDF#) 14-0164) and quartz (SiO_2, PDF# 01-0649) phases from the precursor clay remaining in all samples. The broad diffraction feature between 20° and 35° 2θ is an indication of N-A-S-H gels [50, 51]. Trace amounts of sodium carbonate (Na_2CO_3, PDF#86-295) are formed, either in sampling or testing [52]. A very small amount of a zeolitic phase is also detected, with similar diffraction characteristics to Na-faujasite ($Na_{1.84}Al_2Si_4O_{11.92} \cdot 7H_2O$, PDF#38-238). Faujasite-type phases have been reported many times to be formed in AAMK with a high concentration of sodium (Na/Al≈1), and may transform into zeolites A and P after long-term curing in a warm, humid environment [53]. In this study, the intensity or position of the diffraction hump does not change between any of the dried samples, and the Na-faujasite is still detectable in each of them. These results suggest that the drying procedures do not significantly change the crystallography of AAMK.

(B)

M-mullite
Q-quartz
Z-zeolite (faujasite)
S-[NaAlSi$_3$O$_8$]·xH$_2$O

Q
M
M

M S Q M M M M
Z S Z S Z Z Z M M M Q M M M M Q M M

FD

A50D

105D

65VD

Undried

10   20   30   40   50   60   70   80

2θ (degrees)

(C)

CA
C
Gi

CA-C-A-S-H
C-calcite
HT-hydrotalcite
Gi-gehlenite

HT   C CA   CA   CA   C C CA   CC   C   C
                        Gi C

FD

A50D

105D

65VD

Undried

10   20   30   40   50   60   70   80
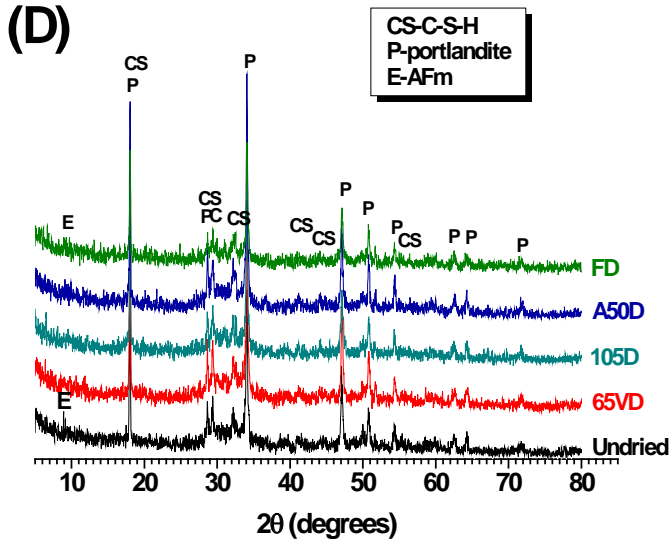
2θ (degrees)

24

Fig.6. XRD patterns of AAC and cement pastes before and after drying: (A) AAMK, (B) AAFA, (C) AAS, and (D) OPC.

In AAFA (Figure 6B), the remaining mullite ($Al_{1.83}Si_{1.08}O_{4.85}$, PDF#89-2645) and quartz (SiO_2, PDF#1-649) from the original fly ash are evident, and a typical broad geopolymer diffraction feature is shown from 20° to 35° 2θ [5]. Trace amounts of faujasite ($Na_{1.84}Al_2Si_4O_{11.92}\cdot 7H_2O$, PDF#38-238) and another hydrous sodium aluminosilicate resembling $[NaAlSi_3O_8]\cdot xH_2O$ (PDF#18-1198) are detected in all the samples, and their diffraction intensities remain almost constant. It was reported that in a sealed container, AAFA that was activated with sodium silicate activator can transform into more ordered structure after 7 days of curing at 80°C [54]. However, there is not any new phase detectible in the dried samples. This is probably due to the rapid water loss in the relatively short period of drying.

AAS (Figure 6C) also exhibits phase stability under the various drying treatments. The main diffraction peak centering at 30° 2θ is attributed to a phase with structure similar to tobermorite ($(CaO)_xSiO_2\cdot zH_2O$, PDF# 10-0374), but known to have substitution of Na and Al. Gehlenite ($Ca_2Al_2SiO_7$, PDF# 35-0755) and calcite ($CaCO_3$, PDF# 47-1743) shown in all the patterns are from the original slag [55], and the carbonation of any remaining pore solution during sampling, respectively. It may be expected that the diffraction intensity of calcite in the A50D sample would be relatively lower than the others because of the full removal of its pore solution (and the ions

25

dissolved in it) by solvent exchange. However, no difference between calcite contents under different drying conditions is evident from the XRD data here.
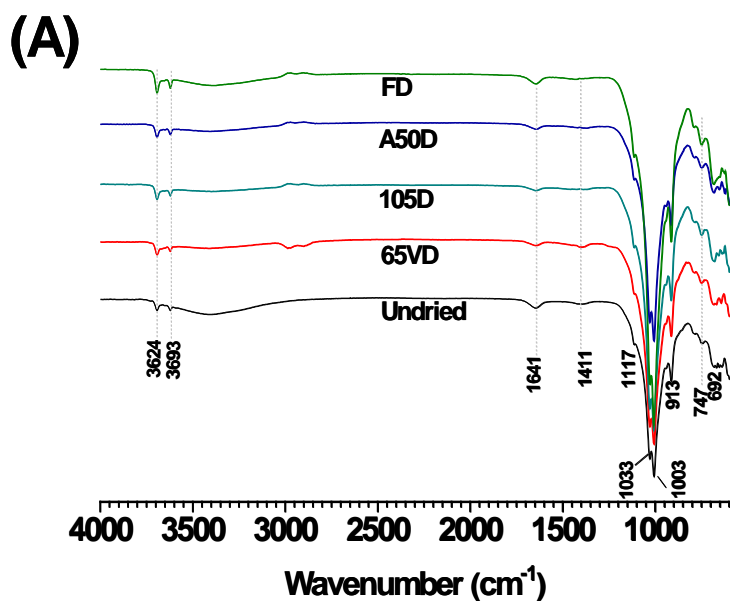
In OPC (Figure 6D), the intensities of characteristic diffraction peaks that belong to calcium silicate hydrate (tobermorite-9Å like structure, $(CaO)_xSiO_2 \cdot zH_2O$, PDF# 10-0374) and portlandite $(Ca(OH)_2$, PDF# 44-1481) remain unchanged. A small amount of AFm phases are detected, and are affected to a limited degree by these drying treatments.
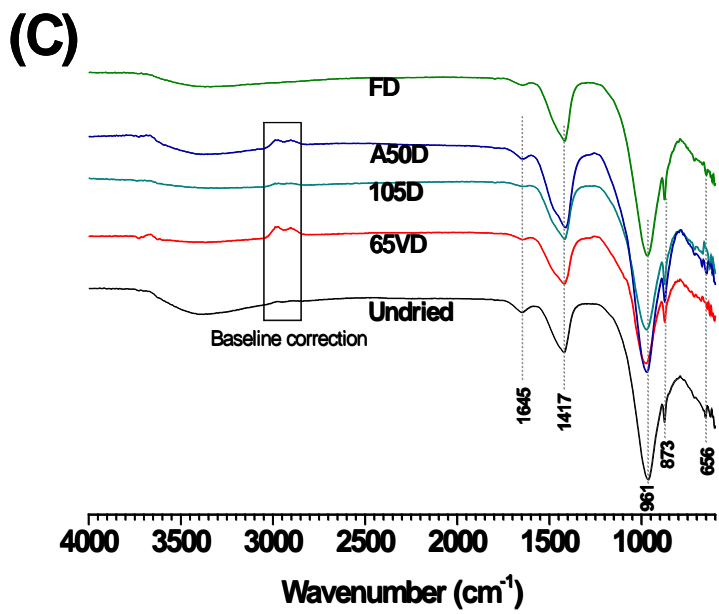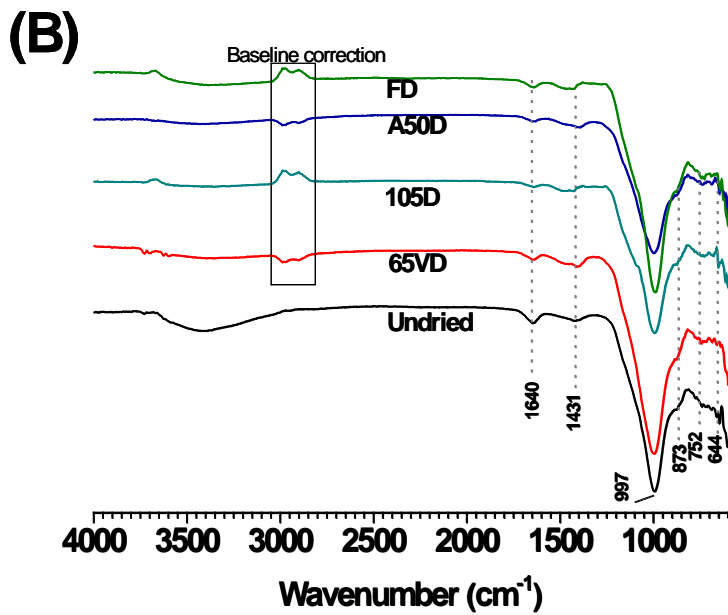
The XRD analysis shows that AAMK and AAFA pastes consist of hydration products with similar structure to zeolites, and these crystalline or semi-crystalline products are stable under the drying conditions. AAS paste consists of hydration products with a similar structure to that which is formed in OPC, and these phases are also unaltered after drying. Since XRD analysis is more effective to detect changes in crystalline phases than disordered ones, and the changes observed by nitrogen sorption seem to be linked to disordered hydrate phases, the effect of the drying procedures on gel phases will be further assessed using FTIR spectroscopy.

3.4 FTIR analysis

Analysis by ATR-FTIR was conducted to examine the effect of drying procedures on the Si(Al)-O and -OH vibration environments; the spectra obtained for all samples are shown in Figure 7. For AAMK, the bands at 692 and 747 cm^{-1} are assigned to Al-O and Si-O vibrations, the band at 913 cm^{-1} is assigned inner -OH bending vibration, and the bands at 1033 and 1117 cm^{-1} is assigned to asymmetric vibration in of Si(Al)-O-Si, and all of them are related to the residual kaolinite [51, 56]. The most intensive band at 1003 cm^{-1} is assigned to the asymmetric stretching of Si(Al)-O-Si in 'geopolymer' networks [50]. The very weak bands at 1411 cm^{-1} in the undried and 65VD samples are assigned to the stretching vibrations of O-C-O bond in carbonate [51], which is in agreement with XRD analysis. The band at 1641 cm^{-1} and the band centered at 3450 cm^{-1} are related to deformation and stretching vibrations of the physically adsorbed water molecules at the surface, respectively [57]. The bands at 3624 and 3693 cm^{-1} are assigned to stretching vibrations of inner hydroxyl group -OH in kaolinite [57]. Except for the reduced intensities of band at 1411 cm^{-1} and 3450 cm^{-1}, which are due to less carbonation and removal of water respectively, the dried samples show the same vibration bands as the undried sample, which confirms that the drying procedures do not affect the structure and environment of Si(Al)-O-Si in AAMK.

For AAFA, the bands at 644 and 752 cm^{-1} are assigned to the vibrations of O-Al, which usually belong to mullite [58]. The bands at 873 and 1431 cm^{-1} are corresponding to out-of-plane bending vibration (v_2) and asymmetric stretching vibration (v_3) of C-O in carbonate [59]. The most intense band at 997 cm^{-1} belongs to the asymmetric stretching of Si(Al)-O-Si in geopolymer network, which is known as a characteristic band to prove the formation of geopolymer [60]. Similar as in AAMK, these bands do not shift after drying. It means that the drying procedures have little effect on the molecular structure of geopolymer and the remaining phases of fly ash. The significantly reduced intensities of bands at 1640 and 3450 cm^{-1} in the dried samples verify the effectiveness of the drying procedures.

(B)

Baseline correction

FD
A50D
105D
65VD
Undried

1640
1431
997
873
752
644

Wavenumber (cm⁻¹)

(C)

FD
A50D
105D
65VD
Undried

Baseline correction

1645
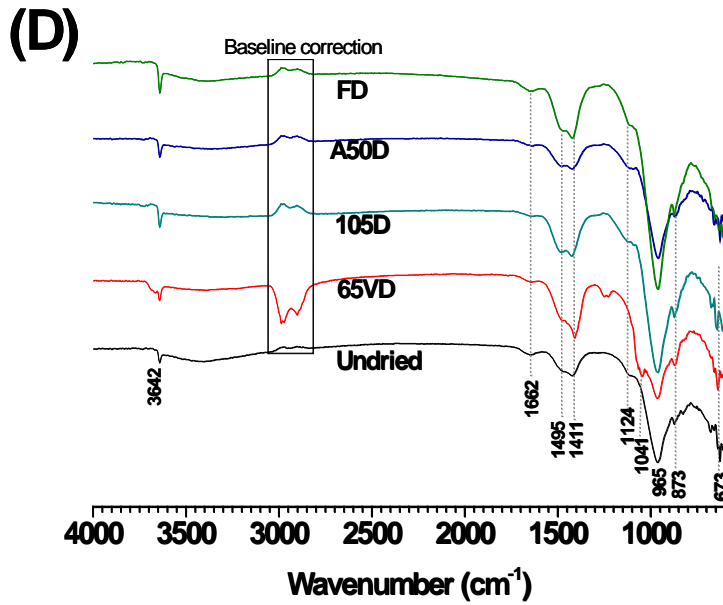1417
961
873
656

Wavenumber (cm⁻¹)

28

Figure 7. ATR-FTIR spectra of pastes: (A) AAMK, (B) AAFA, (C) AAS and (D) OPC.

For AAS, the band at 656 cm^{-1} is assigned to the Si-O-Si bending vibrations in four-membered silicate rings; higher wavenumbers in the range 500-800 cm^{-1} indicate lower polymerization of silicates [46]. The bands and 873 and 1417 cm^{-1} correspond to vibrations of the C-O bond in calcite. The band at 961 cm^{-1} is due to the asymmetric stretching vibration of Si-O-(Si,Al) in the C-A-S-H gel [59]. This vibration band is very sensitive to the gel composition; when Al/Si ratio increases (or decreases), the vibration band shifts to lower (or higher) wavenumbers. The samples show consistent vibration bands at 656 and 961 cm^{-1} before and after drying, which means that the drying procedures did not change the aluminosilicate chain structure in the hydration products.

For OPC, the bands at 673 cm^{-1} is assigned to the Si-O-Si bending vibrations in C-S-H gels with a structure similar to tobermorite [61]. The bands at 873 and 1400-1500 cm^{-1} again correspond to the v_2- and v_3-type of vibrations of CO_3^{2-}. After drying, it is noted that the shoulder at 1495 cm^{-1} is changed, particularly for the FD and 65VD spectra, in which the intensity in this region increases. This means that more carbonate is formed after drying procedures FD and 65VD. The bands at 965 and 1124 cm^{-1} can be assigned to Si–O stretching vibrations of the Q^2 and Q^3 tetrahedra [61]. The spectra 65VD shows a clear shoulder at 1041 cm^{-1}. Finally, the band at 3642 cm^{-1} is assigned to the O–H stretching in portlandite, and its position remains constant. From the spectral shape, and using these data in combination with XRD analysis, it is believed that due to the relatively long

29

drying time of FD and 65VD, the carbonation of the samples leads to minor structural changes in the C-S-H. Carbonation is difficult to avoid in drying and sampling under the conditions adopted in this study, and similarly in many other studies [14, 61]. For the purpose of reducing artificially induced misleading information about the phase, it is wise to choose a less time-consuming process, such as oven or solvent replacement drying.

4. Conclusions

Free water must be removed from cementitious binders prior to characterization in case of pore structure determination by techniques, such as gas adsorption/desorption, as well as MIP and other methods. In this study, we reported the efficiencies of four common drying procedures on alkali-activated cements in comparison with OPC, and their effects on pore measurement by N_2 adsorption and phase determination. We found that the sensitivity of pore and phase structure to drying procedure depends on the nature of the binder. The metakaolin-based and fly ash-based AACs (geopolymers) were less sensitive to drying conditions than the alkali-activated slag and ordinary Portland cement paste. Ethanol replacement drying is the least damaging method for all the pastes studied, and it reached more of the fine pores. We suggest that when two different binders are compared, particularly by measuring their pore structure to interpret their permeability, mass transport characteristics and related durability performance, caution must be taken in selecting and applying the drying procedures before testing. Solvent replacement as a drying technique is more suitable when research focus is on the effect of pore structure as it removes the dissolved species and avoids their consequent chemical effects, while minimizing collapse of the fine pores.

5. Acknowledgements

References

[1] Winnefeld F, Schöler A , Lothenbach B, Chapter 1. Sample preparation, in Scrivener K, Snellings R, Lothenbach B. A Practical Guide to Microstructural Analysis of Cementitious Materials. CRC Press, 2016. pp1-36.

[2] Basheer L, Kropp J, Cleland DJ, Assessment of the durability of concrete from its permeation properties: a review, Construction and Building Materials 15 (2001) 93-103.

[3] Slaty F, Khoury H, Rahier H, Wastiels J, Durability of alkali activated cement produced from kaolinitic clay, Appl. Clay Sci., 104 (2015) 229–237.

[4] Fernandez-Jimenez A, García-Lodeiro I, Palomo A, Durability of alkali-activated fly ash cementitious materials, *J. Mater. Sci.*, 42 (2007) 3055–3065.

[5] Zhu H, Zhang Z. Zhu Y. Tian L. Durability of alkali-activated fly ash concrete: Chloride penetration in pastes and mortars, *Constr. Build. Mater.*, 65 (2014) 51–59.

[6] Yang T, Yao X, Zhang Z, Quantification of chloride diffusion in fly ash-slag-based geopolymers by X-ray fluorescence (XRF), *Constr. Build. Mater.*, 69 (2014) 109–115.

[7] Provis JL, Myers RJ, White CE, Rose V, van Deventer JSJ, X-ray microtomography shows pore structure and tortuosity in alkali-activated binders, Cem. Concr. Res., 42 (2012) 855–864.

[8] Ngala VT, Page CL, Effect of carbonation on pore structure and diffusional properties of hydrated cement pastes, *Cem. Concr. Res.*, 27 (1997) 995-1007

[9] Galle C, Effect of drying on cement-based materials pore structure as identified by mercury intrusion porosimetry A comparative study between oven- , vacuum- , and freeze-drying, *Cem. Concr. Res.*, 31 (2001) 1467–1477.

[10] Zeng Q, Li K. Fen-Chong T, Dangla P, Pore structure characterization of cement pastes blended with high-volume fly-ash, *Cem. Concr. Res.*, 42 (2012) 194–204.

[11] Poon CS, Wong YL, Lam L, The influence of different curing conditions on the pore structure and related properties of fly-ash cement pastes and mortars, *Constr. Build. Mater.*, 11 (1997) 383–393.

[12] Bahador S,   Jong HC, Effect of preconditioning of concrete under accelerated test, in 31st Conference on Our World in Concrete & Structures: 16 - 17 August 2006, Singapore. Article Online Id: 100031015, online version: http://cipremier.com/100031015.

[13] Zhang J, Scherer GW, Comparison of methods for arresting hydration of cement, *Cem. Concr. Res.*, 41 (2011) 1024–1036.

[14] Collier NC, Sharp JH, Milestone NB, Hill J, Godfrey IH, The influence of water removal techniques on the composition and microstructure of hardened cement pastes, *Cem. Concr. Res.*, 38 (2008) 737–744.

[15] Ismail I, Bernal SA, Provis JL, Hamdan S, van Deventer JSJ, Drying-induced changes in the structure of alkali-activated pastes, J. Mater. Sci., 48 (2013) 3566–3577.

[16] Yang K, Yang C, Magee B, Nanukuttan S, Ye J, Establishment of a preconditioning regime for air permeability and sorptivity of alkali-activated slag concrete, Cem. Concr. Compos., 73 (2016) 19–28.

[17] Roy DM, Brown PW, Shi D, Scheetz BE, May W, Concrete microstructure: Porosity and permeability, The Strategic Highway Research Program (SHRP) Report, 1993.

[18] GB/T208-2014, Test method for determining cement density, 2014.

[19] Ma H, Mercury intrusion porosimetry in concrete technology: tips in measurement, pore structure parameter acquisition and application, J. Porous. Mater., 21 (2014) 207–215.

[20] Barrett EP, Joyner LG, and Halenda PP. The determination of pore volume and area distributions in porous substances. I. Computations from nitrogen isotherms. *J. Am. Chem. Soc.*, **73**(1) (1951) 373-80.

[21]   Kuenzel C, Vandeperre LJ, Donatello S, Boccaccini AR, Cheeseman C, Ambient temperature drying shrinkage and cracking in metakaolin-based geopolymers, J. Am. Ceram. Soc., 95 (2012) 3270–3277.

[22] Prud'homme E, Michaud P, Joussein E, Peyratout C, Smith A, Rossignol S, In situ inorganic foams prepared from various clays at low temperature, Appl. Clay Sci., 51 (2011) 15–22.

[23] Zhang Z, Yao X, Zhu H, Hua S, Chen Y, Activating process of geopolymer source material: Kaolinite, J Wuhan Uni. Tech.-Mater. Sci. Ed., 24 (1) (2009) 132–136.

[24] Zhang Z, Provis JL, Reid A, Wang H, Fly ash-based geopolymers: The relationship between composition, pore structure and efflorescence, Cem. Concr. Res., 64 (2014) 30–41.

[25] Ismail I, Bernal SA, Provis JL, San Nicolas R, Hamdan S, van Deventer JSJ, Modification of phase evolution in alkali-activated blast furnace slag by the incorporation of fly ash, Cem. Concr. Compos., 45 (2014) 125–135.

[26] Duxson P, Lukey GC, van Deventer JSJ, The thermal evolution of metakaolin geopolymers: Part 2 - Phase stability and structural development, J. Non. Cryst. Solids, 353 (2007) 2186–2200.

[27] Duxson P, Lukey GC, Van Deventer JSJ, Evolution of gel structure during thermal processing of Na-geopolymer gels, Langmuir, 22(2006) 8750–8757.

[28] Zhou W, Yan C, Duan P, Liu Y, Zhang Z, Qiu X, Li D, A comparative study of high- and low-Al_2O_3 fly ash based-geopolymers: The role of mix proportion factors and curing temperature, Mater. Des., 95 (2016) 63–74.

[29] Bernal SA, Juenger MCG, Ke X, Metthes W, Lothenbach B, De Belie N, Provis JL. Characterization of supplementary cementitious materials by thermal analysis, Mater. Struct., 50:26 (2017).

[30] Provis JL, Harrex RM, Bernal SA, Duxson P, van Deventer JSJ, Dilatometry of geopolymers as a means of selecting desirable fly ash sources, J. Non. Cryst. Solids, 358 (2012) 1930–1937.

[31] Myers RJ, L'Hôpital E, Provis JL, Lothenbach B, Effect of temperature and aluminium on calcium (alumino)silicate hydrate chemistry under equilibrium conditions, Cem. Concr. Res., 68 (2015) 83–93.

[32] Ben Haha M, Lothenbach B, Le Saout G, Winnefeld F, Influence of slag chemistry on the hydration of alkali-activated blast-furnace slag - Part II: Effect of Al_2O_3, Cem. Concr. Res., 42 (2012) 74–83.

[33] Ke X, Bernal SA, Provis JL, Uptake of chloride and carbonate by Mg-Al and Ca-Al layered double hydroxides in simulated pore solutions of alkali-activated slag cement, Cem. Concr. Res., 100 (2017) 1–13.

[34] Lothenbach B, Durdzinski P, De Weerdt K, Chapter 5. Thermogravimetric analysis, in K. Scrivener, R. Snellings, B. Lothenbach. A Practical Guide to Microstructural Analysis of Cementitious Materials, CRC Press, 2016, pp178-208.

[35] Garci Juenger MC, Jennings HM, The use of nitrogen adsorption to assess the microstructure of cement paste, Cem. Concr. Res., 31 (2001) 883–892.

[36] Thiery M, Dangla P, Belin P, Habert G, Roussel N, Carbonation kinetics of a bed of recycled concrete aggregates : A laboratory study on model materials, Cem. Concr. Res., 46 (2013) 50–65.

[37] Melo Neto AA, Cincotto MA, Repette W, Mechanical properties, drying and autogenous shrinkage of blast furnace slag activated with hydrated lime and gypsum, Cem. Concr. Compos., 32 (2010) 312–318.

[38] Yeşilmen S, Al-Najjar Y, Balav MH, Şahmaran M, Yıldırım G, Lachemi M, Nano-modification to improve the ductility of cementitious composites, Cem. Concr. Res., 76 (2015) 170–179.

[39] Knapen E, Cizer O, van Balen K, van Gemert D, Effect of free water removal from early-age hydrated cement pastes on thermal analysis, Constr. Build. Mater., 23 (2009) 3431–3438.

[40] Ben Haha M, Lothenbach B, Le Saout G, Winnefeld F, Influence of slag chemistry on the hydration of alkali-activated blast-furnace slag - Part I: Effect of MgO, Cem. Concr. Res., 41 (2012) 955–963.

[41] Groen JC, Peffer LAA, Perez-Ramirez J, Pore size determination in modified micro- and mesoporous materials . Pitfalls and limitations in gas adsorption data analysis, Microporous Mesoporous Mater., 60 (2003) 1–17.

[42] Bell J, Gordon M, Kriven W, Nano- and Microporosity in Geopolymer Gels, Microsc. Microanal., 12 (2006) no. S02: 552–553.

[43] Zhang Z, Wang H, Zhu Y, Reid A, Provis JL, Bullen F, Using fly ash to partially substitute metakaolin in geopolymer synthesis, Appl. Clay Sci., 88–89 (2014) 194–201.

[44] Zhang Z, Wang H, Yao X, Zhu Y, Effects of halloysite in kaolin on the formation and properties of geopolymers, Cem. Concr. Compos., 34 (2012) 709–715.

[45] Palacios M, Puertas F, Effect of shrinkage-reducing admixtures on the properties of alkali-activated slag mortars and pastes, Cem. Concr. Res., 37 (2007) 691–702.

[46] Lecomte I, Henrist C, Liégeois M, Maseri F,   Rulmont A, Cloots R, (Micro)-structural comparison between geopolymers, alkali-activated slag cement and Portland cement, J. Eur. Ceram. Soc., 26 (2006) 3789–3797.

[47] Bakharev T, Resistance of geopolymer materials to acid attack, Cem. Concr. Res., 35 (2005) 658–670.

[48] Rickard WDA, Williams R, Temuujin J, van Riessen A, Assessing the suitability of three Australian fly ashes as an aluminosilicate source for geopolymers in high temperature applications, Mater. Sci. Eng. A, 528 (2011) 3390–3397.

[49] Zhang Z, Provis JL, Reid A, Wang H, Mechanical, thermal insulation, thermal resistance and acoustic absorption properties of geopolymer foam concrete, Cem. Concr. Compos., 62 (2015) 97–105.

[50] Zhang Z, Provis JL, Wang H, Bullen F, Reid A, Quantitative kinetic and structural analysis of geopolymers. Part 2. Thermodynamics of sodium silicate activation of metakaolin, Thermochim. Acta,   565 (2013) 163–171.

[51] Ozer I, Soyer-Uzun S, Relations between the structural characteristics and compressive strength in metakaolin based geopolymers with different molar Si/Al ratios, Ceram. Int., 41 (2015) 10192–10198.

[52] Cyr M, Pouhet R, Carbonation in the pore solution of metakaolin-based geopolymer, Cem. Concr. Res., 88 (2016) 227–235.

[53] De Silva P, Sagoe-Crenstil K, Medium-term phase stability of Na_2O-Al_2O_3-SiO_2-H_2O geopolymer systems, Cem. Concr. Res., 38 (2008) 870–876.

[54] Ma X, Zhang Z, Wang A, The transition of fly ash-based geopolymer gels into ordered structures and the effect on the compressive strength, Constr. Build. Mater., 104 (2016) 25–33.

[55] Zhang Z, Li L, He D, Ma X, Yan C, Wang H, Novel self-supporting zeolitic block with tunable porosity and crystallinity for water treatment, Mater. Lett., 178 (2016)151–154.

[56] Hoch M, Bandara A, Determination of the adsorption process of tributyltin (TBT) and monobutyltin (MBT) onto kaolinite surface using Fourier transform infrared (FT-IR) spectroscopy, Colloids Surf. A 253 (2005) 117–124.

[57] Kljajević LM, Nenadović SS, Nenadović MT, Bundaleski NK, Todorović BŽ, Pavlović VB, Rakočević ZLj, Structural and chemical properties of thermally treated geopolymer samples, Ceram. Int., 43 (2017) 6700–6708.

[58] Zhang Z, Wang H, Provis JL, Quantitative study of the reactivity of fly ash in geopolymerization by FTIR, J. Sustain. Cem. Mater., 1 (2012) 154–166.

[59]Angulo-Ramírez DE, Mejía de Gutiérrez ., Puertas F, Alkali-activated Portland blast-furnace slag cement: Mechanical properties and hydration, Constr. Build. Mater., 140 (2017) 119–128.

[60] Panias D, Giannopoulou IP, Perraki T, Effect of synthesis parameters on the mechanical properties of fly ash-based geopolymers, Colloids Surfaces A Physicochem. Eng. Asp., 301 (2007) 246–254.

[61] Yu P, Kirkpatrick RJ, Poe B, McMillan PF, Cong X, F, Structure of Calcium Silicate Hydrate (C-S-H): Near-, Mid-, and Far-Infrared Spectroscopy, 82 (1999) 742–748.